Two-Dimensional Fiber Ablation in the Solid-Deuterium Z Pinch

Irvin R. Lindemuth

*Inertial Fusion and Plasma Theory Group, Applied Theoretical Physics Division, Los Alamos National Laboratory,
Los Alamos, New Mexico 87545*

Initial two-dimensional magnetohydrodynamic computer calculations of the formation and evolution of the solid-deuterium-fiber Z pinch are reported. The computations show that the $m=0$ instability occurs very early in the discharge. The $m=0$ behavior leads to the formation of hot spots off axis and enhances the fiber ablation rate. A rapid onset of neutron production occurs when the fiber has totally ablated. The computations are in qualitative agreement with experimental observations at several laboratories and lead to a new interpretation of the experimental diagnostics.

Experiments at Los Alamos,[1-3] the Naval Research Laboratory,[4,5] and Imperial College[6,7] have demonstrated that interesting fusion plasmas can be created by discharging modern high-voltage pulsed power generators through frozen deuterium fibers or solid fibers of other materials. Each institution has developed different diagnostics and each has come to different conclusions about the behavior of fiber-formed pinches. The Naval Research Laboratory (NRL) has interpreted a rapid expansion in visible-light emission, as recorded on a streak photograph, and a rapid onset of neutron production as indicating the onset of the $m=0$ instability, and experimental observations over a range of parameters have led to the hypothesis that fiber-formed plasmas are stable until peak current, i.e., until $dI/dt=0$.[4,5] In contrast, Los Alamos shadowgraph photography shows visible evidence of $m=0$ behavior significantly earlier than peak current.[2,3] Similarly, and perhaps also in contrast with the Los Alamos observations, $m=0$ behavior has been observed at Imperial College at a time very early in the discharge, well before peak current and even prior to the time when the fiber has been completely ionized.[6,7]

This paper reports two-dimensional computations of fiber Z-pinch behavior which are an attempt to reconcile the apparently contrasting experimental observations. The two-dimensional computations reported here are an extension of the previously reported one-dimensional computations[8] which predicted that the presence of a cold, solid central fiber throughout much, if not all, of the duration of the Naval Research Laboratory and Los Alamos experiments may play an important role in the experimental observables and therefore should be considered in any interpretation of the experimental diagnostics. In contrast to recent computational studies of the stability of Z pinches,[9-11] the philosophical approach taken here is to do on a computer an "experiment" which corresponds, as much as feasible, to an actual laboratory experiment. As in the previous study,[8] the computations reported here use "cold-start" initial conditions, a nonideal equation of state, a nonuniform, computed temperature distribution, and a self-consistent

electrical source in an attempt to compute the behavior of a fiber Z pinch from $t=0$. Philosophically similar computations[12] of the laser-initiated, gas-embedded Z pinch[13] were required to reconcile potentially conflicting interpretations of the various diagnostics.[14] The computations reported here are qualitatively consistent with experimental observations and lead to the interpretation that rapid expansion of visible light and onset of neutron production corresponds to complete fiber ablation and not to the onset of instability, which occurs significantly earlier.

The computations reported here use driving conditions approximating the Los Alamos HDZP-I experiment ($V=600$ kV, $I=250$ kA, $\tau_{\text{rise}}=200$ ns) and a 30-μm-diam fiber at half solid density (88 kg/m^3, to account for possible voids and other nonuniformities in the initial fiber), corresponding to the case considered in Figs. 3 and 4 (curve c) of Ref. 8. An initial 2% random density perturbation is superimposed upon the solid fiber, but not upon the low-density, "warm" halo required for current initiation.[8]

Computed density contours in the r-z plane are shown in Fig. 1. Unstable $m=0$ behavior is indicated by non-horizontal contours. The $m=0$ behavior began quite early in the discharge at the outer radial boundary of the hot, coronal plasma which is formed by ablation from the cold, central fiber. The contour values are chosen so that 10% of the total mass lies between each set of adjacent contours, with 50% of the mass within contour e. Hence, even though the $m=0$ instability is well underway, Fig. 1 indicates that approximately half of the mass is still at or above its initial density, and, perhaps more importantly, more than 20% of the mass has expanded to radii significantly larger than the initial fiber radius.

Axial density and temperature profiles on axis are shown in Figs. 2 and 3, respectively. At 35 ns, most of the material on axis has been compressed by a factor of 3 or more (Fig. 2, curve a) and essentially all the material on axis is below 1 eV (Fig. 3, curve a); the $m=0$ behavior in the outer plasma leads to axial nonuniformities much greater than the 2% random initial perturbation.
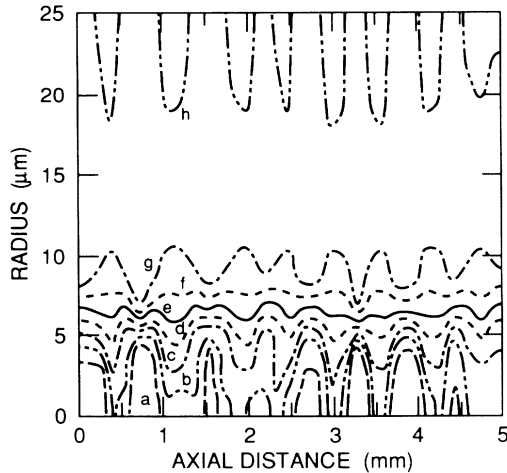
FIG. 1. Mass-density contours in the r-z plane at 25 ns. The contour values are as follows: contour a, 307; b, 266; c, 234; d, 194; e, 155; f, 108; g, 51; h, 0.59 kg/m^3.
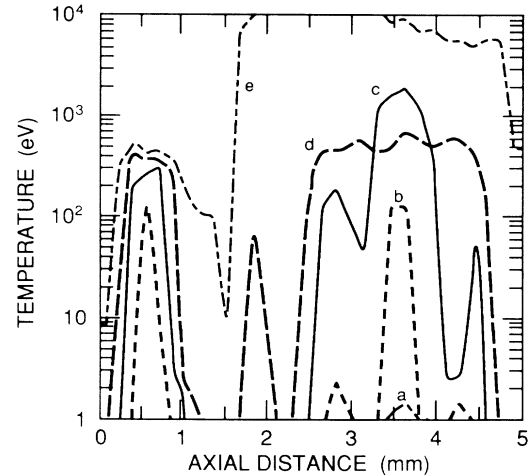

FIG. 3. On-axis axial temperature profiles at the following values of t: curve a, 35 ns; curve b, 40 ns; curve c, 45 ns; curve d, 50 ns; and curve e, 55 ns.

The $m=0$ behavior enhances the fiber ablation rate, and by 45 ns, only approximately one-half of the material on axis remains at high density (Fig. 2, curve c) and the remainder has expanded and reached a relatively high temperature, with some material exceeding the Bennett temperature (Fig. 3, curve c). Complete ionization of the fiber occurs by 55 ns (Figs. 2 and 3, curve e), approximately 10 ns earlier than in the one-dimensional case (Ref. 8, Fig. 3, curve c).

The axial kinetic energy, the thermal energy, the total x-ray emission (300 eV–1 keV), and the neutron production rate based on the computed time-dependent, two-dimensional density and temperature profiles are shown in Fig. 4. The axial kinetic energy (Fig. 4, curve a) shows exponential growth beginning less than 5 ns after

current initiation. By 20 ns, the exponential growth has saturated and thereafter the axial kinetic energy remains at approximately 10%–20% of the total thermal energy (Fig. 4, curve b) of the plasma.

X-ray emission (Fig. 4, curve c) begins at approximately 20 ns and reaches a peak at 40 ns. Most of the emission prior to the minimum at approximately 50 ns occurs off axis in hot spots which occur at the current channel constrictions which result from the $m=0$ behavior. The x-ray emitting regions are shown in Fig. 5; the peak emission is centered at a radius of approximately 60 μm, 4 times larger than the initial fiber radius. The hot spots in the coronal plasma eventually move radially inward, sometimes dividing into two spots which move axially away from each other. The region of peak x-ray
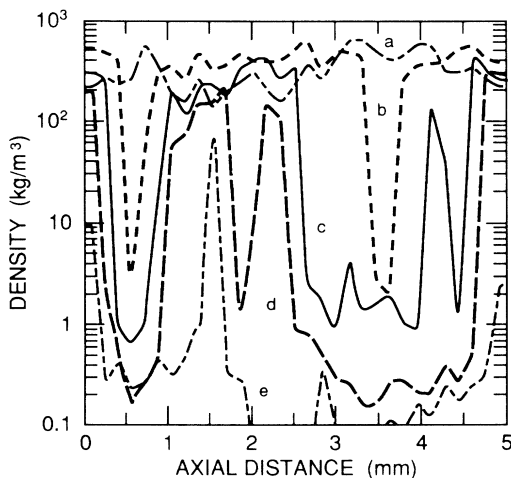

FIG. 2. On-axis axial density profiles at the following values of t: curve a, 35 ns; curve b, 40 ns; curve c, 45 ns; curve d, 50 ns; and curve e, 55 ns.
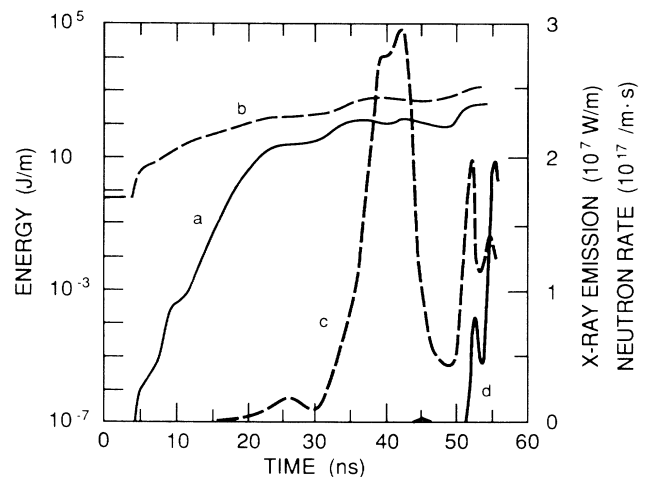

FIG. 4. Curve a, axial kinetic energy; curve b, thermal energy; curve c, x-ray emission; and curve d, neutron production rate, as functions of time. All quantities are per unit length.
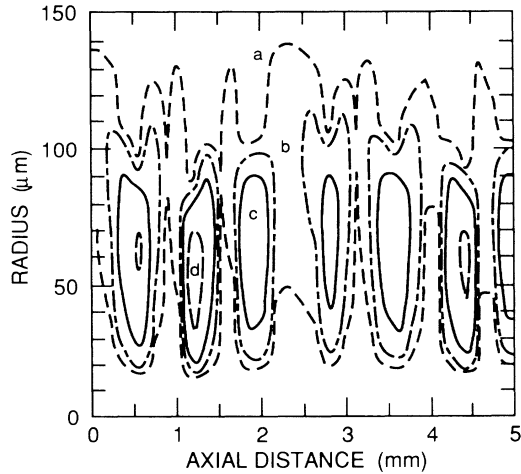
FIG. 5. X-ray emission (300 eV–1 keV) contours in the r-z plane at 20 ns. The contour values are as follows: contour a, 10^{12}; b, 3×10^{12}; c, 10^{13}; d, 3×10^{13} W/m^3.

FIG. 6. Visible emission as a function of time: curve a, average radius inside which 90% of visible emission occurs; curve b, radius at which rate is 10^{12} W/m^3 at $z = 1.25$ mm; curve c, radius at which rate is 10^{12} W/m^3 at $z = 5$ mm.

emission moves to the axis once the cold core on axis has been ablated. The hot spots off axis are consistent with Imperial College observations[7,8] and the subsequent hot spots on axis are consistent with NRL observations.[4,5]

Neutron production (Fig. 4, curve d) occurs abruptly at 50 ns and corresponds to the time of complete fiber ablation on axis (Figs. 2 and 3, curves c, d, and e). The rapid onset of neutron production, with a rise time of approximately 5 ns, is consistent with NRL observations.[4] Because of numerical difficulties, the computations have not been carried out far enough to compute a neutron pulse width and total yield. The peak rate, if sustained for 20 ns, would give a total yield of 2×10^8 neutrons, which is somewhat higher than reported by Los Alamos[1–3] and somewhat less than reported by NRL.[4,5] The onset of neutron production occurs earlier than reported by Los Alamos, perhaps because of the sub-solid-density used in the initial condition. The neutron production rate is significantly higher than would be attained in the corresponding one-dimensional computation and supports our previous conjecture[8] that McCall's mechanism,[15] which predicts the neutron yield scaling of the NRL experiment, would not apply until the fiber has totally ablated.

Even in the one-dimensional computations,[8] the final disappearance of the cold solid fiber removes the on-axis heat sink which the cold material represents and changes the temperature profile. The changing temperature profile is reflected in part by emitted light. Figure 6 shows the temporal behavior of emitted light based on the computed density and temperature profiles. On the average (Fig. 6, curve a), visible light is confined to radii less than 100 μm until complete fiber ablation is approached, at which time there is a rapid expansion, similar to that reported by NRL.[4,5] Because the changing
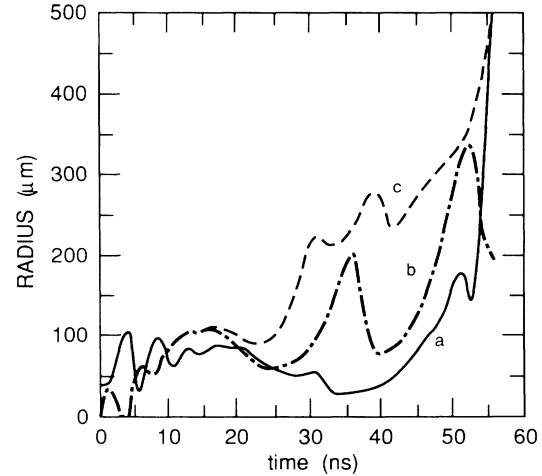
total visible emission rate makes interpretation of Fig. 6 (curve a) somewhat ambiguous, the radius at which the visible emission rate is 10^{12} W/m^3, generally more than 2 orders of magnitude less than the peak emission rate, is also shown in Fig. 6 (curves b and c) for two different axial locations. In each case, a rapid increase in radius occurs as fiber ablation is approached. At other axial locations (i.e., other lines of sight), curves corresponding to Fig. 6 (curves b and c) show a decrease in radius and even a disappearance of visible emission as the plasma heats and expands, phenomena apparently not yet observed at NRL.

Although computational considerations (axial and radial dimensions of the computational mesh, number of computational cells, initial conditions, driving source, physical model, equation of state, and transport-coefficient uncertainties, etc.) may preclude a more detailed agreement, the computations reported here represent comprehensive qualitative agreement with observations reported by several different laboratories. The computations reported here lead to a new interpretation of the behavior of fiber-formed pinches. According to the computations, unstable $m = 0$ behavior begins very early (Fig. 4, curve a) in the discharge, prior to complete ionization of the fiber, in the coronal plasma which forms outside the cold central core. The $m = 0$ behavior leads to enhanced fiber ablation rates and enhanced expansion of the plasma ablated from the fiber. The early-time behavior is indicated by x-ray emission off axis in the coronal region (Fig. 5). Ultimately, the material on axis is transformed into plasma, and densities and temperatures high enough to produce significant neutron yield are attained. Neutron production (Fig. 4, curve d), on-axis x-ray production (Fig. 4, curve c), and rapidly expanding visible light (Fig. 6) signify complete fiber ablation, not

181

the onset of unstable $m = 0$ behavior. Unstable $m = 0$ behavior begins significantly earlier than neutron production. Based upon the results reported here, the ultimate utility of the long-lived fiber-formed Z pinches in a fusion context becomes not merely the relatively simple question of stability or lack thereof but, rather, the more complex question of the implications of long-time evolution of unstable behavior.

Computations using a significantly shorter axial length (e.g., 300 μm) show[16,17] some qualitative differences with the computations reported here, most likely because the shorter length limits the longest wavelength to which the $m = 0$ behavior, which originally starts at the shortest wavelength the computational mesh can support, can cascade. The effect of this limit is presently being studied.

The authors of Refs. 10 and 11 are correct to question the conjectures of Ref. 8, which have been confirmed here, because of the different operating conditions under which the NRL $dI/dt = 0$ hypothesis appears to hold. Two-dimensional computations using NRL parameters have been initiated,[16,17] but numerical difficulties and computational expense have so far precluded carrying out these computations through peak current. Whether or not such computations will confirm the interpretation of this paper must await subsequent research.

A laser-ray-tracing algorithm developed by Glasser and Lovberg[18] is being applied to the computations reported here to determine when the early-time $m = 0$ behavior predicted here would become visible in shadowgram photography.

[1]D. W. Scudder, Bull. Am. Phys. Soc. **30**, 1408 (1985).

[2]J. Hammel and D. W. Scudder, in *Proceedings of the Fourteenth European Conference on Controlled Fusion and Plasma Physics, Madrid, Spain, 1987,* edited by F. Engelmann and J. L. Alvarez Rivas (European Physical Society, Petit-Lancy, Switzerland, 1987), p. 450.

[3]J. Hammel, in *Dense Z-Pinches,* edited by N. R. Pereira, J. Davis, and N. Rostoker (American Institute of Physics, New York, 1989), p. 303.

[4]J. D. Sethian, A. E. Robson, K. A. Gerber, and A. W. DeSilva, Phys. Rev. Lett. **59**, 892 (1987); **59**, 1790(E) (1987).

[5]J. D. Sethian, A. E. Robson, K. A. Gerber, and A. W. DeSilva, in *Dense Z-Pinches* (Ref. 3), p. 308.

[6]M. G. Haines, J. Bailey, P. Baldock, A. R. Bell, J. P. Chittenden, P. Choi, M. Coppins, I. D. Culverwell, A. E. Dangor, E. S. Figuera, and G. J. Rickard, in *Proceedings of the Twelfth International Conference on Plasma Physics and Controlled Nuclear Fusion Research, Nice, France, 1988* (IAEA, Vienna, 1989), Paper No. C-4-4-2.

[7]E. S. Figuera, G. H. McCall, and A. E. Dangor (to be published).

[8]I. R. Lindemuth, G. H. McCall, and R. A. Nebel, Phys. Rev. Lett. **62**, 264 (1989).

[9]A. H. Glasser and R. A. Nebel, in *Dense Z-Pinches* (Ref. 3), p. 226.

[10]F. L. Cochran and A. E. Robson, Phys. Fluids B **2**, 123 (1990).

[11]I. D. Culverwell and M. Coppins, Phys. Fluids B **2**, 129 (1990).

[12]I. R. Lindemuth, J. H. Brownell, T. A. Oliphant, and D. L. Weiss, J. Appl. Phys. **53**, 1415 (1982).

[13]L. A. Jones, K. H. Finken, A. Dangor, E. Kallne, S. Singer, I. R. Lindemuth, J. H. Brownell, and T. A. Oliphant, Appl. Phys. Lett. **38**, 522 (1981).

[14]I. R. Lindemuth, in *Proceedings of the First International Conference on Dense Z-Pinches for Fusion,* edited by J. D. Sethian and K. A. Gerber (Naval Research Laboratory, Washington, DC, 1984), p. 46.

[15]G. H. McCall, Phys. Rev. Lett. **62**, 1986 (1989).

[16]I. R. Lindemuth, in *Dense Z-Pinches* (Ref. 3), p. 327.

[17]I. R. Lindemuth, in Proceedings of the Fifth International Conference on Megagauss Magnetic Field Generation and Related Topics, Novosibirsk, USSR, 1989 (to be published).

[18]A. H. Glasser and R. Lovberg (private communication).